ADVANCED OPTICAL MATERIALS
www.advopticalmat.de

Tracking Exciton Diffusion and Exciton Annihilation in Single Nanoparticles of Conjugated Polymers by Photon Correlation Spectroscopy

*Jakob Schedlbauer, Sabrina Streicher, Michael Forster, Ullrich Scherf, Jan Vogelsang, and John M. Lupton**

A fundamental question relating to the nature of light emission and absorption in organic semiconductors is the dimension of the domain within a bulk material responsible for the interaction of light and matter. How large can a nanoparticle become to retain the quantized nature of light emission? Excitons are only a few nanometers in size, but because they diffuse in space, they probe a much larger volume than the single molecule. When excitons meet, they may decay non-radiatively by singlet–singlet or singlet–triplet annihilation (SSA or STA). Fluorescence photon statistics reveal whether single photons are emitted (photon antibunching) or arrive in randomly spaced packets (photon bunching), offering direct insight into excitonic mobility. Single multichain nanoparticles of ladder-type poly(para-phenylene) (LPPP) are examined. The effect of SSA and STA is seen in the photon antibunching and bunching, respectively, which both decrease in fidelity as the size of the nanoparticle increases. Time resolving the photon correlation measurement yields microscopic annihilation rates for SSA and STA in agreement with values obtained from bulk LPPP films. Even though triplets in LPPP are known to be highly mobile, the results show that, on the timescale of the singlet exciton lifetime, triplet diffusion is not of significance in the STA process.

1. Introduction

One of the appeals of organic electronics is that the optoelectronic functionality is mostly monomolecular in nature. The emission color of an organic light-emitting diode (OLED), for example, arises primarily from the electronic structure of the individual molecular building block making up the thin film of the device, implying that single-molecule fluorescence techniques are ideal probes of the underlying intrinsic electronic structure.[1] Intermolecular interactions can, conceivably, arise between polymer chains, inducing H- and J-type aggregation effects,[2] but such coupling is usually effectively suppressed by resorting to molecules with bulky sidechains.[3] A π-conjugated polymer material that has proven particularly interesting in this regard is ladder-type poly(para-phenylene) (LPPP).[4] This compound not only displays a remarkable structural rigidity, minimizing excited-state relaxation and therefore making absorption and luminescence spectra near-perfect mirror images of each other.[5] It also shows well-resolved vibronic transitions, attesting to the low degree of intermolecular disorder. Interchain electronic aggregation effects are virtually absent, so that ensemble absorption and emission spectra are almost identical in the dissolved form and in bulk films.[5] In fact, intermolecular interactions are so weak that the sum of single-molecule luminescence spectra almost perfectly replicates the bulk-film ensemble spectrum.[6] At the same time, LPPP-based materials have a high fluorescence quantum yield and exhibit substantial photostability, making them ideal for applications involving large excitation densities.[5] Feldmann and Lemmer pioneered the use of LPPP in low-threshold mechanically flexible laser structures,[7] a feat that received widespread attention culminating in the award of the Philip-Morris Research Prize.[8] To this day, a photograph of the far-field intensity pattern generated by such a plastic laser[9] decorates the cover of the journal "Organic Electronics".[10] More recently, the unique characteristics of LPPP have been exploited in optical microcavities to create exciton-polariton condensates by strong light–matter coupling,[11] which can even enable optical transistor-like action[12] and single-photon optical nonlinearities at room temperature.[13]

Inferring polymer aggregation effects from spectral signatures alone can be challenging and requires a detailed understanding

J. Schedlbauer, S. Streicher, J. Vogelsang, J. M. Lupton
Institut für Experimentelle und Angewandte Physik and Regensburg Center for Ultrafast Nanoscopy (RUN)
Universität Regensburg
Universitätsstrasse 31, 93040 Regensburg, Germany
E-mail: john.lupton@ur.de
M. Forster, U. Scherf
Macromolecular Chemistry Group
Chemistry Department and Wuppertal Center for Smart Materials and Systems (CM@S)
Bergische Universität Wuppertal
Gauss-Strasse 20, 42097 Wuppertal, Germany

DOI: 10.1002/adom.202200092

of the complete photophysics of the isolated chain.[14] In phenylene-vinylenes, for example, spectral broadening and a loss of vibronic structure can arise even in single oligomers, which cannot fold back on themselves to form aggregates.[15] This spectral diversity of the individual chromophoric unit is related to the high degree of flexibility of the π-conjugated segment as confirmed by molecular dynamics simulations.[16] Bent chromophores tend to be associated with broad, featureless PL spectra, whereas straight units are characterized by narrow-band electronic transitions with a well-defined vibronic progression.[17] In contrast, the LPPP chromophore is generally straight.[18] Although, unlike some other conjugated polymers, LPPP does not form electronic interchain aggregates (spectral signatures initially attributed to aggregation effects[19] were later found to arise from oxidative on-chain luminescent defects[20]), it can still be coaxed into a physical aggregate to form discrete multichain nanoparticles.[21] A range of different routes to nanoparticle growth have been discussed in the literature, such as the miniemulsion approach used to stabilize nanoparticles formed by sonication,[21,22] but most research has focused on structural investigations of these objects rather than on optical spectroscopy of single particles.[23] To address this lack of understanding, we have introduced a versatile method of growing single polymer nanoparticles from single chains by carefully controlled solvent-vapour annealing (SVA), allowing the particle growth to be tracked in situ.[24] Here, single chains are dispersed in a polymethylmethacrylate (PMMA) matrix, which is subsequently swelled by a mixture of solvents. Since the solubilities of the PMMA host and the guest polymer molecules differ, aggregation of the polymers can be driven by the solvent ratio and the duration of the swelling process. Under a fluorescence microscope, the number of diffraction-limited luminescent spots—corresponding to the number of individual polymer chains—can simply be counted, offering a precise metric for the size of the polymer nanoparticle formed by SVA and the number of polymer chains contained in it.[25] This technique has proven to be particularly powerful in examining nanoparticles of poly(para-phenylene-butadiinylene) (PPEB), which tend to form H-type electronic aggregates.[25,26] This electronic coupling is revealed by strong spectral shifts from the single-chain transitions, a loss of vibronic structure, and an order-of-magnitude increase in photoluminescence (PL) lifetime. In addition, a striking correlation between the PL lifetime and the spectral redshift has been demonstrated in model dimers and trimers of cofacially placed chromophores:[27] as the coupling strength rises, the red-shift increases and the transition oscillator strength is suppressed. Crucially, such electronic aggregation can be shown to be a reversible process. Careful swelling of the polymer nanoparticle within the PMMA matrix removes the spectral signatures of H-type aggregation but retains the overall shape and structure of the particle.[26]

A polymer chain can contain multiple chromophores,[6] and a polymer nanoparticle can contain multiple chains. It is therefore of great interest to understand how these chromophores interact with one another, even if they do not form electronic aggregates. Excitation energy can hop between the chromophores.[28] However, when two excitons are present within the aggregate, one can pass its excitation energy to another and is thereby "annihilated". If the excited-state absorption of one chromophore overlaps spectrally with the excited-state emission of another, and the two excited states are spaced no further apart than the Förster radius of excitation energy transfer, singlet–singlet annihilation (SSA) occurs.[29] As a consequence of SSA, even a multichromophoric polymer chain or a multichain aggregate can exhibit deterministic single-photon emission in the PL. This "antibunching" of photons is characterized by the fluctuations in the stream of the emitted photons, measured by fluorescence correlation spectroscopy.[30] Studies of the variation of photon antibunching with nanoparticle size offer a metric of assessing the excitonic diffusion length, on the nanometre scale.[31] Such exciton diffusion is a critical parameter in organic photovoltaic devices since it relates to both exciton splitting and parasitic carrier recombination losses. The single-photon microscopic approach discussed in the following is entirely complementary to conventional measurements of exciton diffusion by time-resolved fluorescence quenching by electron acceptors, such as those pioneered by Feldmann and Lemmer.[32]

Excitation energy in a molecular aggregate can also be removed non-radiatively by triplet excited-state species, since the triplet state also gives rise to a specific absorption band. In this case of singlet–triplet annihilation (STA),[33] the nanoparticle will remain non-emissive for the duration of the triplet lifetime, which, depending on the structure of the molecule involved and the temperature, can be hundreds of microseconds. The influence of such STA, even in single LPPP chains, is readily seen by the fact that the PL intensity is generally increased under exposure to molecular oxygen, which quenches the excited-state triplets, returning the polymer to the singlet ground state.[34]

Bimolecular recombination between two excitons is a critical effect in optoelectronic devices. Under high excitation densities, SSA has long been known to arise in laser waveguide structures, competing with, or even entirely suppressing, the optical gain effect.[35] SSA in conjugated polymers may be so pronounced that it can even show up in a transition from a linear to a square-root-type dependence of the PL intensity on excitation fluence.[36] In addition, STA is the main mechanism preventing continuous-wave lasing in organic semiconductors, since more and more long-lived triplets build up in the material during prolonged excitation due to the finite intersystem crossing from the excited singlet state S_1 to the triplet state T_1.[37] This effect has been resolved directly in a laser structure based on an LPPP derivative, where the phosphorescence from the triplet state was found to be suppressed by stimulated emission depletion of the singlet excited state above the lasing threshold, thus lowering the overall yield of intersystem crossing.[38] In an OLED, on the other hand, where the dominant excited-state species is the triplet exciton, even at comparatively low excitation densities, STA can limit the overall quantum efficiency, leading to a roll-off at higher drive currents.[39] At the same time, however, two triplet excitons may also annihilate, giving rise to delayed fluorescence which raises the overall efficiency again.[39]

The interplay between STA and SSA in LPPP nanoparticles is non-trivial since the triplet exciton also has a certain degree of mobility within the polymer. This mobility is readily seen in the fact that a small concentration of heavy-metal atoms, less

than one such contaminant per polymer chain,[20c] is sufficient to activate the phosphorescence channel in OLEDs made of the polymer due to the local spin-orbit coupling induced. The effect, which can be exploited to study spin dynamics, such as electron spin precession in nuclear hyperfine fields and the associated magnetoresistance,[40] and test quantitatively for singlet fission effects,[41] arises because of the high diffusion length of the triplet excitons, which migrate to the emissive metal-atom sites.[42] It is therefore of interest to study the STA and SSA rates in LPPP nanoparticles as a function of size to establish whether it is only the singlet excitons that diffuse or whether triplet motion on the timescale of the singlet lifetime is also of significance.

Here, we demonstrate the growth and spectroscopy of individual LPPP nanoparticles comprising a well-defined number of single polymer chains. We identify the exciton diffusion and annihilation dynamics by considering both photon bunching and antibunching, and probe the transition between on-chain and interchain exciton diffusion kinetics in nanoparticles of different sizes. By resolving the photon correlation signal in time,[31] that is, by selecting photons of prompt and slightly delayed emission, we arrive at quantitative estimates for the rates of STA and SSA, which agree well with those obtained with conventional ensemble spectroscopy. In contrast to ensemble spectroscopy, however, the single-particle approach offers a truly microscopic visualization of exciton migration on the nanoscale—rather than conventional far-field ensemble-based techniques[43]—as well as probing the transition from the intrinsic single-chain characteristics to the features of the bulk film.

2. Experimental Approach

In our experiment we directly measure the time it takes for two excitations—either two singlet excitons or one singlet and one triplet exciton—to diffuse inside each other's FRET radius and subsequently annihilate. These two processes are illustrated in **Figure 1**a. In the top left panel, two S_1 singlet excitons (blue discs) are generated by pulsed laser excitation, and start to diffuse inside the polymer nanoparticle. After a certain time following excitation, Δt_{SSA}, both excitons come close to each other and annihilate, leading to the emission of a single photon—photon antibunching occurs. In the right-hand side panel, one singlet exciton and one T_1 triplet exciton (black disc) are depicted. Again, a certain time following excitation, Δt_{STA}, both excitons come close to each other and S_1 is annihilated by T_1, leading to an interruption of the photon stream for a duration of the lifetime of T_1—photon bunching occurs. Previously, the diffusivity of singlet excitons in LPPP was measured to be roughly three orders of magnitude higher than that of triplets.[32,44] We illustrate this in the figure as T_1 being comparatively immobile during the singlet exciton lifetime.

Figure 1b shows a sketch of the underlying experiment to extract Δt_{SSA} and Δt_{STA}. We split the fluorescence of a single nanoparticle onto two avalanche photodiodes using a semitransparent mirror in order to calculate the coincidence rate of consecutively detected photons as a function of their arrival time difference $\Delta\tau$ between both detectors. In the case of a perfect single-photon emitter, it is impossible to detect two

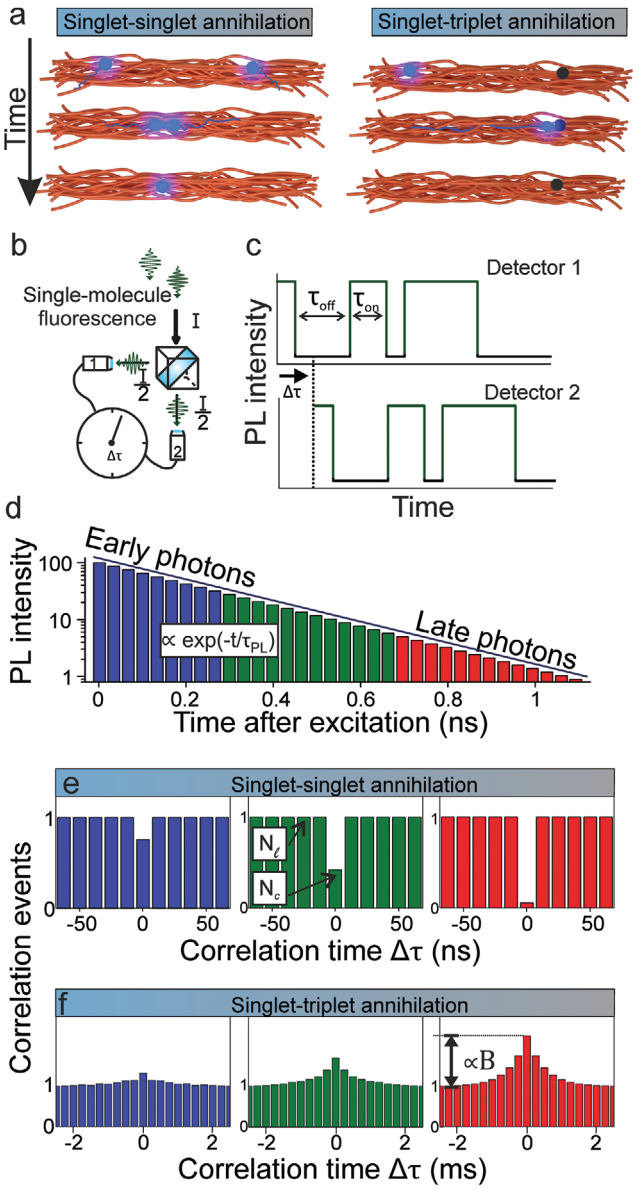

Figure 1. Time-resolved photon correlation measurements of conjugated-polymer nanoparticles. a) Sketch of the time evolution of bimolecular annihilation between singlet (blue discs) and triplet (black discs) excitons. b) The single-molecule fluorescence is split equally by a semitransparent mirror and detected by two single-photon counting modules. c) Illustration of the correlation analysis. Excursions to a dark state result in a characteristic blinking signature in the PL intensity recorded on both detection channels. Average lengths durations of "on-" and "off-" periods τ_{on} and τ_{off} can be analyzed by calculating the cross-correlation between both channels as a function of the correlation time $\Delta\tau$. d) Sketch of the distribution of photon arrival times, which decreases exponentially with time according to the PL lifetime. e) Photon correlation histograms for correlation times on the nanosecond timescale calculated for intervals of increasing photon arrival times (left to right). The colors correspond to those used in (d). Photon antibunching is quantified in terms of the ratio of central to lateral peaks in the histogram, N_c/N_ℓ. f) Photon correlation histograms for correlation times on the millisecond timescale calculated for intervals of increasing photon arrival times (left to right). The colors correspond to those used in (d). Photon bunching is quantified in terms of the bunching amplitude B at zero delay time. The decrease of N_c/N_ℓ, that is, the photon antibunching dip in (e) and the increase of the photon bunching amplitude B in (f) report on the time evolution of SSA and STA, respectively.

photons after one single excitation pulse.[45] Binning the correlation signal in intervals of the inverse laser repetition rate as illustrated in Figure 1e reveals a strongly reduced central correlation amplitude at an arrival-time difference of zero, an effect referred to as photon antibunching. Calculating the ratio between the central and lateral values of this correlation histogram, N_c/N_ℓ, directly reports on the average number of independent emitters N, with $N = \frac{1}{1-N_c/N_\ell}$.[46] When multiple chromophores contribute to the PL signal, antibunching can only be observed if the SSA rate is high compared to the photoluminescence rate. On longer timescales, the opposite behavior can be seen in the correlation histogram if intermittent excursions to a long-lived dark state quench the fluorescence as indicated in Figure 1c. This fluorescence "blinking" behavior gives rise to a pronounced signature of photon bunching that decays exponentially with increasing correlation time (Figure 1f). The bunching amplitude B, given by the ratio between the central level of the correlation histogram at $\Delta\tau = 0$ and the number of correlation events on long timescales, is directly related to the on- and off-times τ_{on} and τ_{off}. These values correspond to the mean times during which the molecule emits a continuous photon stream or resides in a dark state, respectively. As before, in multichromophoric systems, the magnitude of photon bunching depends on the strength of STA compared to the photoluminescence rate. If singlet-exciton annihilation by triplets occurs on timescales much longer than the PL lifetime, the correlation curve will be flat, that is, $B \to 1$.

It has been shown previously how consideration of the "microtime" of each photon detected, that is, the time between the incident excitation pulse and the detection of a fluorescence photon, can resolve exciton–exciton annihilation directly in the time domain.[31] Figure 1d–f sketches the basic idea underlying the data analysis. The distribution of microtimes recorded within the photon stream decays exponentially over time with the PL rate $k_{PL} = \tau_{PL}^{-1}$ as sketched in Figure 1d on a logarithmic scale. Calculating the photon correlation for a specific microtime window, for example considering only photons with low (blue bars), intermediate (green bars) or large (red bars) microtimes, monitors SSA and STA over time. For early photons, the time available for annihilation to occur is too short and therefore only weak signatures of antibunching and bunching are identifiable in the photon correlation (Figure 1e,f, blue histograms). When choosing photons with large microtimes, the probability for SSA and STA increases, which reflects in a strong decrease of $\frac{N_c}{N_\ell}$ (for the case of SSA) and a strong increase of B (for the case of STA). The calculation of these microtime-dependent quantities, that is, $N \to N(t) = \frac{1}{1-N_c(t)/N_\ell(t)}$ and $B \to B(t)$, therefore offers direct access to the SSA and STA rates. Following the procedure of Hedley and coworkers,[31] we fit $N(t)$ using the expression

$$N(t) = \left\{\gamma_0 - \left[A \times \exp\left(-k_{SSA} t\right)\right]\right\}^{-1} \quad (1)$$

where k_{SSA} is the rate for SSA, $1/(\gamma_0 - A)$ the number of independent emitters at time zero, and $1/\gamma_0$ the final number of emitters after SSA.[31]

In order to extract the STA rate, we start by considering the previously reported analytical treatment of the microtime independent bunching amplitude B which is given by[33]

$$B = \frac{\tau_{off}}{\tau_{on}} \left(\frac{1-f}{1+\frac{\tau_{off}}{\tau_{on}} f} \right)^2 + 1 \quad (2)$$

where $f = \frac{F_1}{F_2}$ is the ratio of intensities with (F_1) and without (F_2) a triplet exciton present in the nanoparticle. This ratio can be written in a time-dependent form as

$$f \to f(t) = \frac{F_1(t)}{F_2(t)} = \frac{I_0 \times \exp\left\{-\left(k_{PL} + k_{STA}\right) \times t\right\}}{I_0 \times \exp\left\{-\left(k_{PL}\right) \times t\right\}} = \exp\left(-k_{STA} \times t\right) \quad (3)$$

Here, k_{PL} is the PL rate, k_{STA} the STA rate, and I_0 the initial number of excitations. With this analysis, we can express the time-dependent bunching amplitude $B(t)$ as a function of the STA annihilation rate as

$$B(t) = B_0 \left(\frac{1-\exp\left(-k_{STA} \times t\right)}{1+B_0 \times \exp\left(-k_{STA} \times t\right)} \right)^2 + 1 \quad (4)$$

with $B_0 = \frac{\tau_{off}}{\tau_{on}}$.

Figure 2a shows the chemical structure of the LPPP derivative used here, phenyl-substituted LPPP (PhLPPP, R = phenyl). The compound was dissolved in toluene and further diluted into a 2 wt% PMMA/toluene solution before spin coating onto a cleaned borosilicate microscope slide. We used a confocal microscope to scan over a sample area of 20 × 20 μm^2, from which we extracted the spot density (molecules/area). To grow conjugated polymer aggregates we treated the sample by using solvent vapor annealing as described elsewhere.[24a,26,47] SVA leads to a swelling of the PMMA matrix allowing the single molecules to freely diffuse and agglomerate. By comparing the spot densities before and after SVA as shown in Figure 2b we can reliably estimate the average aggregate size, that is, the average number of polymer chains per nanoparticle.

3. Results

We performed measurements on single nanoparticles of three different sizes as well as on single chains. Figure 2c–f shows spectra of isolated single molecules as well as of small, medium, and large aggregates. The average particle sizes are 1, ≈10, ≈40, and ≈110 chains/particle as determined by counting the number of fluorescent spots per unit area before and after solvent vapor annealing.[24a,25,26] For simplicity, we label these four samples as S for single chain, and A_S, A_M, and A_L for small, medium, and large aggregates. Single-chain spectra show a strong 0–0 transition at close to 460 nm, and weaker vibronic peaks at 490 and 525 nm. A distinct scatter of the transition energy is visible since the 0–0 peak positions vary between 455 and 465 nm.

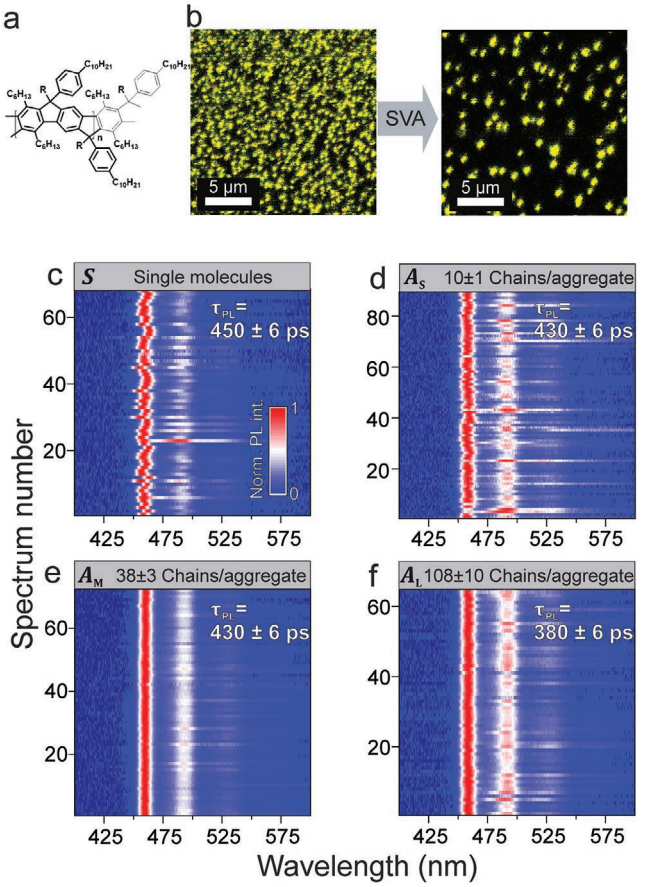

Figure 2. Single-aggregate formation and fluorescence spectroscopy. a) Chemical structure of the conjugated polymer LPPP (R = methyl for MeLPPP or R = phenyl for PhLPPP). b) Confocal fluorescence microscope scan images of a sample area of PhLPPP before (left) and after (right) annealing the sample in a solvent vapour. Calculating the spot densities of both images allows the aggregate size to be estimated as described in the methods section. c–f) 2D-plots of single-particle PL spectra for PhLPPP aggregates of different sizes. The average aggregate size is stated on the top of each plot along with the average PL lifetime.

Upon aggregation this scatter in the PL spectra disappears and particularly in A_M and A_L we observe little variation of the 0–0 peak energy between single particles. The average PL lifetimes are stated in the panels and show little dependency on the particle size. Both the PL lifetime measurement and the spectral analysis demonstrate that no interchain electronic coupling, that is, H-type aggregation, arises in PhLPPP following nanoparticle formation. Because the underlying electronic structure of the excited state does not change, we can therefore probe both SSA and STA while only changing the particle size.

We begin by measuring the degree of photon antibunching in **Figure 3**a for all four samples as shown by photon coincidence histograms integrated over all microtimes. To eliminate the possibility of multiple excitations during a single laser pulse, the pulse width of the excitation source used must be short compared to the PL lifetime.[45] Therefore, we excited the nanoparticles with a frequency-doubled femtosecond Ti:sapphire laser operating at a wavelength of 405 nm with a pulse width of 215 fs. The average N_c/N_ℓ ratios are stated as insets in each panel. Single PhLPPP chains show virtually perfect single photon emission with a coincidence ratio of $\frac{N_c}{N_\ell} = 0.05$. As described previously, this value translates to a number of independent emitters of $N = 1.05$.[46] Upon increasing the nanoparticle size by aggregation, N_c/N_ℓ also increases up to $\frac{N_c}{N_\ell} = 0.63$ (i.e., $N = 2.7$) for the largest aggregate sample, A_L. To extract the SSA rate we calculate the number of independent emitters $N(t)$ as a function of photon arrival time in steps of 25 ps as plotted in Figure 3b. In sample S the $N(t)$ curve is constant over the first 500 ps, showing a value of $N(t) \approx 1$. Upon aggregation we observe a higher initial value of $N(t = 0)$ of ≈2, ≈5, and ≈11 for A_S, A_M, and A_L, respectively. The data are fitted by Equation (1) and the extracted SSA rates are stated in the figure. Because no time dependence of $N(t)$ is visible for sample S we cannot determine k_{SSA} for these sample, but we estimate a lower limit for the SSA rate as stated in the figure. Nevertheless, we observe a strong decrease of k_{SSA} by at least one order of magnitude down to $k_{SSA} = (4 \pm 1) \times 10^9\ s^{-1}$ in A_L.

The PL quenching by triplet excitons leads to a pronounced photon bunching amplitude on longer timescales of the photon correlation curve. **Figure 4**a shows the photon correlation signal integrated over all microtimes for the four samples on a semilogarithmic scale. The thin gray lines represent correlation curves calculated from single nanoparticles whereas the thick gray line is the median correlation curve. After the calculation of the correlation curves for different photon arrival times, the bunching amplitude $B(t)$ is extracted for different times after excitation and plotted in Figure 4b. In sample S the amplitude $B(t)$ is constant over time and, crucially, has a finite value of $B(t) > 1$. This situation changes in the aggregated samples and $B(t)$ increases significantly for later photon arrival times. Fitting the data in Figure 4b with Equation (4) reveals a strong decrease of k_{STA} from $k_{STA} \geq 100 \times 10^9\ s^{-1}$ for single chains down to $k_{STA} = (1.5 \pm 0.2) \times 10^9\ s^{-1}$ in A_L. The rates extracted for each sample are stated in the figure.

4. Discussion

To compare our results obtained from microtime-resolved photon statistics with values reported previously in the literature, the mere annihilation rates are not a suitable metric. These numbers state the average time needed for two excitons within a volume V to undergo annihilation. Hence the interaction volume increases with an increasing number of molecules within one aggregate, and so the observed reduction of the annihilation rates with increasing aggregate size is expected. In contrast, a calculation of the bimolecular annihilation coefficient γ_{Ann} gives a measure of the effective strength of annihilation within the material by renormalizing the rates measured to the interaction volume V. In general, any kind of annihilation process contributes to the nonradiative decay of singlet excitons and therefore decreases the singlet exciton density ρ_S over time.[48] The decrease of the singlet density due to annihilation for a given type of annihilation, that is, STA or STA, is then given by

$$\frac{d}{dt}\rho_S(t)|_{Ann} = -\gamma_{Ann} \times \rho_{Ann}(t) \times \rho_S(t) \quad (5)$$

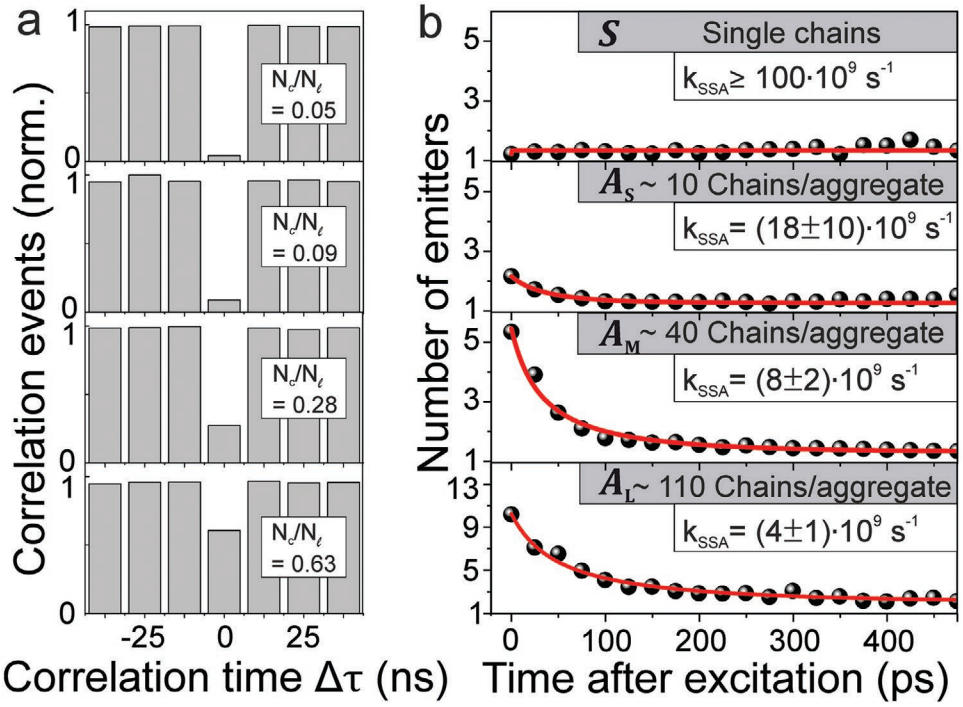

Figure 3. Temporal evolution of photon antibunching in the photon statistics as a function of photon detection time, the microtime. a) Averaged photon correlation histograms for single PhLPPP particles of increasing size (top to bottom) on the nanosecond timescale. The photon coincidence peak ratios N_c/N_ℓ extracted from the histograms are stated explicitly. b) Dependence of the number of emitters extracted from the photon correlation measurement on the time of photon detection, that is, on the time after excitation (black points). The data are fitted by Equation (1) (red lines). The SSA rates extracted from these fits are stated in the diagrams.

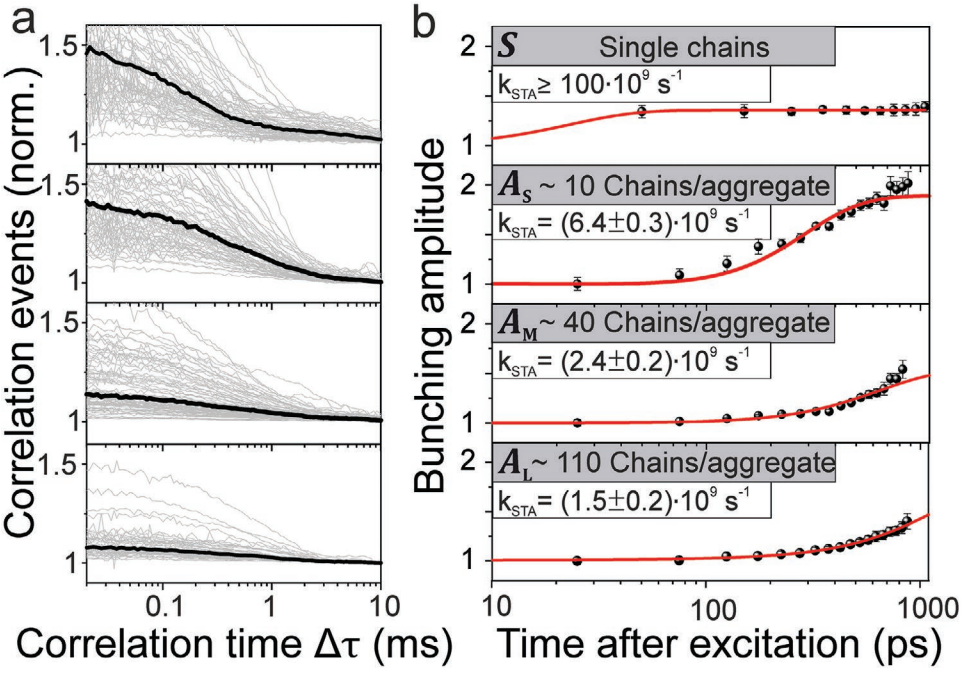

Figure 4. Temporal evolution of photon bunching in the photon correlation as a function of microtime. a) Photon correlation curves for single PhLPPP nanoparticles (thin grey lines) of increasing size (top to bottom) on the millisecond timescale, plotted on a semilogarithmic scale together with the median correlation curves (thick gray lines). b) Dependence of the correlation amplitude *B* on photon microtime after excitation (black points). The data were fitted by Equation (4) (red lines). The extracted rates for STA are stated in the diagrams.

Table 1. Dependency of the bimolecular annihilation coefficient on the aggregate size for SSA and STA. The errors include the measurement uncertainties in both the determination of the annihilation rates themselves and the size of the nanoparticles studied. The last row gives literature values.[32,50]

Sample	Number of chains/particle	Annihilation coefficient for SSA [10^{-9} cm^3 s^{-1}]	Annihilation coefficient for STA [10^{-9} cm^3 s^{-1}]
A_S	10 ± 1	4.0 ± 2	1.4 ± 0.2
A_M	38 ± 3	6.7 ± 2	2.0 ± 0.3
A_L	108 ± 10	9.6 ± 3	3.6 ± 0.8
Literature value MeLPPP[32,50]		4.2	0.57

Here, ρ_{Ann} denotes either the exciton density of triplets or singlets depending on the annihilation process described. A singlet exciton is annihilated following the annihilation rate k_{Ann}, which is connected to γ_{Ann} by[31,48]

$$\gamma_{Ann} = \frac{k_{Ann}}{\rho_{Ann}} = k_{Ann} \times \frac{V}{n_{Ann}} \quad (6)$$

Here, V is the volume of the nanoparticle carrying n_{Ann} annihilation partners, that is, excitons. Considering the molecular mass of ≈15 kDa of the PhLPPP compound used in this study and using the average mass density of 1.1 g cm^{-3}[49] we can estimate the volume of the aggregates as described in the Experimental Section. The excitation rate in the single particle measurements is typically two orders of magnitude smaller than the repetition rate of the laser, that is, far below saturation.[45] The situation that two excitons are generated after one laser pulse is therefore a rare event. However, monitoring the coincidence rate of two consecutively detected photons in the correlation analysis offers a very sensitive pathway to probing these events. To a reasonable first approximation, the number of annihilation partners available for any given singlet exciton is therefore $n_{Ann} = 1$. We calculate γ_{Ann} for SSA and STA and give the result for each aggregate size in **Table 1**. In addition, we compare our results with previously reported values of LPPP films, which are given in the last row of Table 1.[32,50] We find excellent agreement between the literature values of the SSA coefficient in bulk films of MeLPPP and our datasets. Within the experimental error, $\gamma_{Ann,\,SSA}$ is virtually independent of aggregate size, showing an average value of $\gamma_{Ann,SSA} = 6.8 \times 10^{-9}$ cm^3 s^{-1}. We measure an average annihilation coefficient for STA of $\gamma_{Ann,STA} = 2.3 \times 10^{-9}$ cm^3 s^{-1}. Because the reported value of $\gamma_{Ann,STA} = 0.57 \times 10^{-9}$ cm^3 s^{-1} is measured at a temperature of 80 K rather than at room temperature, our observation of a fourfold stronger $\gamma_{Ann,STA}$ can be rationalized by the increased exciton mobility at higher temperatures.[51] We also observe a slight increase of $\gamma_{Ann,STA}$ with increasing particle size, up to a value of $\gamma_{Ann,STA} = 3.6 \times 10^{-9}$ cm^3 s^{-1}, which at first glance is not expected. We note, however, that it has been shown that the fluorescence anisotropy of conjugated polymers can be larger than the corresponding anisotropy in absorption, which indicates that energy migration toward certain emissive sites occurs.[52] Such a directional energy migration would tend to concentrate all the excitons on a few emissive sites within the nanoparticle aggregate, thereby lowering the effective interaction volume. In other words, a random diffusion of excitons cannot be assumed anymore. Therefore, the calculation of $\gamma_{Ann,STA}$ using the actual physical volume of the particles will lead to an overestimation particularly in the case of larger aggregates. Another explanation would be that interchain exciton diffusion is more pronounced in larger aggregates compared to the intrachain exciton diffusion which dominates in smaller aggregates and in single chains. An important observation lies in the fact that $\gamma_{Ann,STA}$ is smaller by a factor of three compared to $\gamma_{Ann,SSA}$, which implies that triplets are not mobile in the STA process.

It is important to note that, even though single PhLPPP chains exhibit a well-defined triplet lifetime and show a single-exponential photon correlation function, triplet excitons can also be quenched by photogenerated charge carriers.[53,54] Upon the formation of a polaron during the measurement of a single LPPP chain, the time periods showing singlet-polaron quenching (SPQ) or triplet-polaron quenching (TPQ) can be clearly distinguished from each other as we demonstrated previously: SPQ is signified by a complete suppression of the PL intensity and TPQ by a vanishing of the photon bunching correlation amplitude.[53b] However, the efficiency of these quenching processes decreases in a multichain nanoparticle in a way comparable to the decrease seen for SSA and STA. Therefore, a clear distinction between different measurement periods from the PL intensity trace either with (TPQ) or without (no TPQ) a polaron present is not strictly possible anymore, preventing an assignment of a well-defined dark-state lifetime to the photon correlation function. SPQ also influences the time scale on which the correlation function decays, further complicating the determination of the triplet lifetime.

Unfortunately, the photon correlation technique can only provide a lower limit for the SSA rate since the single PhLPPP chains always show perfect photon antibunching,[45] even for the photons with the earliest arrival times. For the time-resolved photon bunching measurements, the data hint at the possibility of some dynamics arising in the bunching amplitude for the single-chain measurement (Figure 4b), although this deviation from a flat line is still within the experimental error. If the signal quality can be improved upon further, for example by longer sampling times or accumulation of larger datasets, it may become possible to differentiate between on-chain and interchain STA processes. For on-chain STA, one could conceivably anticipate additional dynamics in the bunching amplitude because of on-chain triplet diffusion. Detailed studies of triplet diffusion in model donor-bridge-acceptor structures by transient absorption spectroscopy have indicated that slow multistep hopping of triplets can be accompanied by swift single-step tunneling.[55] Such rapid kinetics of triplet excitations are also seen in the striking nanosecond phosphorescence dynamics of PhLPPP, which follows a power-law rather than an exponential decay with time.[44,56]

Finally, it is worth contrasting our observations regarding photon bunching and STA in PhLPPP nanoparticles, which do not show signatures of electronic aggregation, with aggregates of other conjugated polymer materials. The most striking electronic aggregation effects have been reported for PPEB-based materials, which can form both interchain H-type species but also give rise to intrachain J-type coupling under physical aggregation.[26] In this polymer, the fluorescence is strongly quenched upon H-type aggregation so that single-particle measurements have to be performed in air with ambient oxygen present, which quenches the triplet population. As a consequence, no photon bunching is seen in the PL of single H-type aggregated PPEB nanoparticles. However, if the interchain coupling is removed, for example by swelling the single particle by SVA, a finite photon bunching amplitude returns, even under oxygen conditions.[26] At the same time, the high degree of chain ordering lends the polymer PL J-type aggregation characteristics with decreased linewidths, transition lifetimes, and vibronic intensities.[26] Since the triplet population should be quenched by oxygen, it is conceivable that long-lived charge-carrier pair states are formed in this case, facilitated by the original triplet formation. Such a process has indeed been reported for rhodamine dye molecules.[57] The carrier-pair dark state in J-type PPEB aggregates appears to be shorter lived than the regular triplet excited state, so that the time scale of the photon bunching amplitude in the photon correlation measurement amounts only to a few microseconds.[26] This situation is very different to the present case of PhLPPP aggregates, where we find the triplet dark-state lifetime in the photon correlation measurement to be of the order of 500 μs. Also, as seen in Figure 4, long-lived dark states are apparent for all particle sizes. In contrast, in poly(3-hexylthiophene) (P3HT), a polymer studied widely because of its utility in photovoltaics, the opposite effect is observed. Intersystem crossing and triplet dark-state formation is particularly efficient in single P3HT chains, leading to a nonradiative decay of almost every second photon by STA.[58] The longer the chains, the more light is absorbed, the greater the excitation rate and therefore the sooner a transition to the dark state occurs. The lifetime of the dark state, however, is independent of chain length on the single-chain level, implying that the localized triplet exciton is not influenced by the remainder of the chain.[58] However, in single nanoparticle aggregates, this STA effect is suppressed entirely, even though strong photon antibunching can still be observed from the nanoparticle, implying efficient interchain SSA.[59] The conclusion of these observations is that, in P3HT, the triplet is quenched in multichain aggregates. It has been suggested that the energetics of the P3HT system is such that the localized intramolecular triplet exciton can directly populate interchain charge-transfer states in multichain aggregates.[60] This mechanism clearly is not at play in the PhLPPP aggregates under investigation here, where triplet shelving, STA, and photon bunching are retained even in large particles. We note that the unusual energetics of P3HT is quite apparent in the fact that the single-chromophore PL transitions can span almost 0.8 eV in energy,[61] whereas those of LPPP are localized to within 30 meV.[62] Because of this energetic heterogeneity in P3HT, it is not possible to infer the occurrence of electronic aggregation effects in P3HT based merely on the PL spectrum.[61]

5. Conclusion

Exciton diffusion and annihilation are key processes that define optoelectronic materials and have therefore been studied extensively in bulk materials. Here, we have introduced a method based on photon correlation spectroscopy to extract information about such processes in nanometre sized particles. A detailed analysis provides information about singlet and triplet diffusion and SSA and STA, respectively, allowing these important processes to be correlated with the microscopic structure, a feat which is not easily accomplished in bulk measurements. We applied this method to a ladder-type conjugated polymer, PhLPPP, which does not show any sign of electronic interchain coupling, making it an ideal candidate for our study. We find that the larger the particle, the lower the annihilation rates become, both in terms of SSA and STA, as interchain exciton diffusion becomes more important. Further, SSA and STA coefficients follow very similar trends with particle size, implying that both are limited by the singlet diffusivity. By comparing these results with our work on P3HT,[59] it may seem surprising that different conjugated polymer materials exhibit such differences in terms of the photon statistics. This diversity is related both to the morphology of the single chain and the nanoparticle, the proximity of interchain contact, but also to the overall energetics of the excited states. The most striking observation is that the STA mechanism is clearly retained in multichain PhLPPP nanoparticles but suppressed in P3HT nanoparticles, presumably because charge formation occurs in the latter. The study of the optical properties of single polymer nanoparticles offers non-trivial insight into the way single polymer chain arrange to ultimately form a bulk film.

Finally, we remark that the original motivation for using the PhLPPP derivative in this study was to identify signatures of triplet quenching by the Pd atoms responsible for enabling room-temperature phosphorescence in this material.[44] Since photon bunching is preserved throughout, even, on average, in large aggregates, we conclude that triplets are not noticeably depopulated by swift intersystem crossing enabled by the metal atom. The short-lifetime phosphorescence in this material must therefore arise from triplets diffusing on length scales much longer than those relevant here. Such large volumes, however, cannot be probed by the methodology presented here since they exceed the singlet diffusion length in size. Singlet diffusion and subsequent annihilation is the prerequisite for observing both photon antibunching and photon bunching,[58,59] so if the interaction of triplets with the metal centers only becomes relevant for much larger particles, there will be no effect on the photon statistics. Elemental analysis of PhLPPP has indicated a Pd concentration of ≈80 ppm,[20c] which, for the given molecular weight, would correspond to an upper estimate of approximately one atom per 90 polymer chains. Assuming that not all Pd atoms contribute to intersystem crossing and phosphorescence, the true density of effective metal sites is likely to be much smaller, making it quite improbable that triplet quenching can be observed in the photon statistics.

6. Experimental Section

Sample Preparation: The synthetic procedure and further information about the ladder polymer LPPP used was reported

elsewhere.[4,20] The molecular weight of the PhLPPP compound used was M_w = 19 600 g mol^{-1} and M_n = 14 700 g mol^{-1}. In addition to the dataset presented here, a methyl-substituted LPPP compound MeLPPP with a molecular weight of M_w = 51 100 g mol^{-1} and M_n = 26 000 g mol^{-1} was also used to grow polymer nanoparticles of different sizes. These MeLPPP aggregates showed similar results with respect to the PL lifetime, the PL spectrum, and the degree of photon bunching and antibunching as the PhLPPP discussed in the main text. The PhLPPP molecules were dissolved in toluene and further diluted to ≈1 pM concentration and mixed with a 2 wt% PMMA/toluene solution. The mixture was spin coated onto cleaned borosilicate cover slips resulting in single isolated PhLPPP molecules within a PMMA matrix of ≈100 nm thickness. Glass substrates were cleaned by sonicating them in a 2% Hellmanex II (Hellma Analytics)/water mixture for 30 min. After drying with nitrogen, the glass slips were treated in a UV-ozone cleaner (Novascan: PSD Pro Series UV) for 1 h. Blank PMMA samples were checked for fluorescent contaminations prior to each measurement.

Experimental Setup: The experimental setup consisted of a confocal microscope (Olympus IX71) with a high N.A. oil immersion objective (Olympus: UPLSAPOX N.A. = 1.35). A frequency doubled Ti:sapphire laser (Spectra-Physics: MaiTai-BB) provided the excitation laser beam at a wavelength of 405 nm with a repetition rate of 80 MHz. The pulse lengths at the sample position was measured to be ≈215 fs.[45] The excitation polarization was set to be circularly polarized to obtain the same excitation probability for each measured spot independent of the orientation of the transition dipole moment of the single polymer chains and nanoparticles within the PMMA film. The excitation density for measurements on single molecules, and on small, medium, and large nanoparticles, was set to 400, 150, 150, and 30 Wcm^{-2}, respectively, reflecting the increased absorption cross section for the larger objects. The emitted photon stream was detected using two single-photon counting modules (Picoquant: MPD-050-CTB) connected to a TCSPC timing device (Picoquant: HydraHarp400). Single particle spectra were acquired using a spectrograph (Andor Technology plc.: SR-303i-B) coupled to a CCD camera (Andor Technology plc.: DU401A-BV). The exposure time was set to 3 s for each spectrum. Measurements were performed under ambient conditions, where triplets were quenched by oxygen, except for the measurements regarding STA. To stabilize the triplet state in this case, the samples were incorporated in a gas flow cell and measured under a constant flow of 100 sccm (standard cubic centimeter per minute) of nitrogen to avoid triplet quenching by molecular oxygen present in the ambient air.

Solvent-Vapour Annealing: Fabrication of the polymer nanoparticles was carried out by treating the PhLPPP/PMMA film with SVA for a time period of 30 min with a fixed solvent ratio of acetone and chloroform.[24a,25] This was achieved by purging nitrogen with a fixed flow rate through two solvent reservoirs containing dry acetone and chloroform. The flow rates were adjusted by two mass flow controllers (MKS instruments) and set to be 7 and 3 sccm for acetone and chloroform, respectively. Subsequently, the nitrogen/solvent stream was combined and used to anneal a sample area of ≈1 cm^2. After SVA, samples were exposed to a constant nitrogen flow of 100 sccm for 20 min to dry them. To vary the size of the nanoparticles, the density of single chains per area was subsequently increased before SVA. To reliably estimate the spot density for high concentrations, the density of a sample with a relatively low spot density of 0.31 ± 0.01 molecules μm^{-2} was first measured. Subsequently, three different samples were fabricated by increasing the concentration of PhLPPP within the PhLPPP/toluene/PMMA solution prior to spin coating by factors of 5, 20, and 100. In order to ensure a linear dependency of the spot densities on concentration prior to SVA the sample preparation was performed, that is, spin coating for all samples with the same parameters while only increasing the PhLPPP concentration in the PhLPPP/toluene/PMMA solution. In addition, for each LPPP concentration multiple samples were fabricated in order to exclude systematic variations induced by the spin coating process, which was prone to handling uncertainties. After SVA, the spot densities of the three samples were measured to be 0.150 ± 0.008, 0.165 ± 0.005, and 0.288 ± 0.013 nanoparticles μm^{-2}. The average number of chains per nanoparticles therefore corresponds to 10 ± 1, 38 ± 3, and 108 ± 10. Using the molecular weight of M_n = 14 700 g mol^{-1} and assuming an average mass density of 1.1 g cm^{-3}[49] the average volume taken by a single PhLPPP chain was calculated to be 2.44 × 10^{-20} cm^3. By multiplying this value with the average number of chains the volume of the nanoparticles was calculated.

Data Analysis: PL spectra of single nanoparticles were background corrected, normalized, and are shown in Figure 2 without further processing. The recorded intensity transients of single nanoparticles were analyzed up until the time when a major irreversible bleaching event occurs. PL lifetimes were obtained by fitting a single exponential decay to the microtime histogram measured for each particle, calculated from photons detected during the first 0.5 s of the measurement. Oxidation is known to lead to emissive keto defects in LPPP nanoparticles,[20b] which is also visible in the measurements presented here. Therefore, single nanoparticles showing this kind of defect formation, which was visible in a sudden increase of the PL lifetime above 1 ns and a redshifted emissive feature at ≈560 nm, were excluded from the analysis. Nevertheless, the observed variations in the relative intensities of the 0–1 transition in Figure 2c–f are most likely related to a small amount of residual defect emission overlapping the 0–1 transition, which appeared to be most pronounced in both A_S and A_L. The basic principle of the microtime-resolved correlation analysis is sketched in Figure 1. To perform this analysis, the microtime was first set at the peak of the instrument response function of this setup to zero. To estimate the microtime-dependent bunching amplitude $B(t)$ photons within a certain microtime window were selected on both detection channels and used to calculate the correlation histogram. Due to the limited photostability and emission rate of the nanoparticles the resulting histograms had to be averaged over multiple single particles. Applying a single-exponential fit returned the bunching amplitude at each position of the microtime window. The curves plotted in Figure 4b show the median values calculated for ≈100 nanoparticles of each size. For time-resolved antibunching measurements, an analogous analysis was performed except for one difference. Here, the photon pairs contributing to the microtime integrated histograms in Figure 3a were filtered by the arrival time of only the first detected photon, independently of the second one.[31] This analysis did not change the resulting curve of $N(t)$ compared to selecting both photons within a certain microtime window, but it increased the number of coincidences and therefore the data quality. By following this procedure, photon antibunching histograms were accumulated over multiple nanoparticles and the number of emitters was calculated as a function of the microtime.

Acknowledgements

The authors thank Prof. Jochen Feldmann for piquing interest in bimolecular recombination phenomena in conjugated polymers. The authors are grateful for collaborative funding provided by the Deutsche Forschungsgemeinschaft (DFG, project number 466652575). J.V. is indebted to the Deutsche Forschungsgemeinschaft for funding through Grant No. 470075523. The authors thank Dr. Felix Hofmann for providing the artwork shown in Figure 1a.

Open access funding enabled and organized by Projekt DEAL.

Conflict of Interest

The authors declare no conflict of interest.

Data Availability Statement

The data that support the findings of this study are available from the corresponding author upon reasonable request.

Keywords

conjugated polymers, exciton annihilation, exciton diffusion, photon statistics, single-particle spectroscopy

Received: January 14, 2022
Revised: May 3, 2022
Published online: June 22, 2022

[1] J. M. Lupton, *Adv. Mater.* **2010**, *22*, 1689.
[2] N. J. Hestand, F. C. Spano, *Chem. Rev.* **2018**, *118*, 7069.
[3] J. M. Lupton, I. D. W. Samuel, R. Beavington, P. L. Burn, H. Bässler, *Adv. Mater.* **2001**, *13*, 258.
[4] U. Scherf, K. Müllen, *Makromol. Chem.* **1991**, *12*, 489.
[5] B. Schweitzer, G. Wegmann, D. Hertel, R. F. Mahrt, H. Bässler, F. Uckert, U. Scherf, K. Müllen, *Phys. Rev. B* **1999**, *59*, 4112.
[6] F. Schindler, J. Jacob, A. C. Grimsdale, U. Scherf, K. Müllen, J. M. Lupton, J. Feldmann, *Angew. Chem., Int. Ed.* **2005**, *44*, 1520.
[7] C. Kallinger, M. Hilmer, A. Haugeneder, M. Perner, W. Spirkl, U. Lemmer, J. Feldmann, U. Scherf, K. Müllen, A. Gombert, V. Wittwer, *Adv. Mater.* **1998**, *10*, 920.
[8] Philip Morris Forschungspreis, https://de.wikipedia.org/wiki/Philip_Morris_Forschungspreis#1999 (accessed: December 2021).
[9] S. Riechel, C. Kallinger, U. Lemmer, J. Feldmann, A. Gombert, V. Wittwer, U. Scherf, *Appl. Phys. Lett.* **2000**, *77*, 2310.
[10] Organic Electronics, https://www.journals.elsevier.com/organic-electronics (accessed: December 2021).
[11] J. D. Plumhof, T. Stöferle, L. J. Mai, U. Scherf, R. F. Mahrt, *Nat. Mater.* **2014**, *13*, 247.
[12] A. V. Zasedatelev, A. V. Baranikov, D. Urbonas, F. Scafirimuto, U. Scherf, T. Stöferle, R. F. Mahrt, P. G. Lagoudakis, *Nat. Photonics* **2019**, *13*, 378.
[13] A. V. Zasedatelev, A. V. Baranikov, D. Sannikov, D. Urbonas, F. Scafirimuto, V. Y. Shishkov, E. S. Andrianov, Y. E. Lozovik, U. Scherf, T. Stöferle, R. F. Mahrt, P. G. Lagoudakis, *Nature* **2021**, *597*, 493.
[14] T. Q. Nguyen, V. Doan, B. J. Schwartz, *J. Chem. Phys.* **1999**, *110*, 4068.
[15] B. J. Schwartz, *Nat. Mater.* **2008**, *7*, 427.
[16] K. Becker, E. Da Como, J. Feldmann, F. Scheliga, E. T. Csanyi, S. Tretiak, J. M. Lupton, *J. Phys. Chem. B* **2008**, *112*, 4859.
[17] a) J. M. Lupton, *ChemPhysChem* **2012**, *13*, 901; b) T. Adachi, J. Vogelsang, J. M. Lupton, *J. Phys. Chem. Lett.* **2014**, *5*, 2165; c) P. Wilhelm, J. Vogelsang, G. Poluektov, N. Schönfelder, T. J. Keller, S. S. Jester, S. Höger, J. M. Lupton, *Angew. Chem., Int. Ed.* **2017**, *56*, 1234; d) P. Wilhelm, J. Vogelsang, N. Schönfelder, S. Höger, J. M. Lupton, *Phys. Rev. Lett.* **2019**, *122*, 057402.
[18] a) J. G. Müller, M. Anni, U. Scherf, J. M. Lupton, J. Feldmann, *Phys. Rev. B* **2004**, *70*, 035205; b) J. G. Müller, J. M. Lupton, J. Feldmann, U. Lemmer, U. Scherf, *Appl. Phys. Lett.* **2004**, *84*, 1183.
[19] U. Lemmer, S. Heun, R. F. Mahrt, U. Scherf, M. Hopmeier, U. Siegner, E. O. Göbel, K. Müllen, H. Bässler, *Chem. Phys. Lett.* **1995**, *240*, 373.
[20] a) J. M. Lupton, *Chem. Phys. Lett.* **2002**, *365*, 366; b) L. Romaner, G. Heimel, H. Wiesenhofer, P. S. de Freitas, U. Scherf, J. L. Brédas, E. Zojer, E. J. W. List, *Chem. Mater.* **2004**, *16*, 4667; c) J. M. Lupton, A. Pogantsch, T. Piok, E. J. W. List, S. Patil, U. Scherf, *Phys. Rev. Lett.* **2002**, *89*, 167401.
[21] K. Landfester, R. Montenegro, U. Scherf, R. Güntner, U. Asawapirom, S. Patil, D. Neher, T. Kietzke, *Adv. Mater.* **2002**, *14*, 651.
[22] M. C. Baier, J. Huber, S. Mecking, *J. Am. Chem. Soc.* **2009**, *131*, 14267.
[23] a) J. Pecher, S. Mecking, *Chem. Rev.* **2010**, *110*, 6260; b) D. Tuncel, H. V. Demir, *Nanoscale* **2010**, *2*, 484; c) A. Kaeser, A. Schenning, *Adv. Mater.* **2010**, *22*, 2985; d) L. H. Feng, C. L. Zhu, H. X. Yuan, L. B. Liu, F. T. Lv, S. Wang, *Chem. Soc. Rev.* **2013**, *42*, 6620.
[24] a) J. Vogelsang, T. Adachi, J. Brazard, D. A. V. Bout, P. F. Barbara, *Nat. Mater.* **2011**, *10*, 942; b) J. Vogelsang, J. M. Lupton, *J. Phys. Chem. Lett.* **2012**, *3*, 1503; c) J. Yang, H. Park, L. J. Kaufman, *Angew. Chem., Int. Ed.* **2018**, *57*, 1826; d) T. W. Tseng, H. Yan, T. Nakamura, S. Omagari, J. S. Kim, M. Vacha, *ACS Nano* **2020**, *14*, 16096.
[25] T. Stangl, P. Wilhelm, K. Remmerssen, S. Höger, J. Vögelsang, J. M. Lupton, *Proc. Natl. Acad. Sci. USA* **2015**, *112*, E5560.
[26] T. Eder, T. Stangl, M. Gmelch, K. Remmerssen, D. Laux, S. Höger, J. M. Lupton, J. Vogelsang, *Nat. Commun.* **2017**, *8*, 1641.
[27] a) C. Allolio, T. Stangl, T. Eder, D. Schmitz, J. Vogelsang, S. Höger, D. Horinek, J. M. Lupton, *J. Phys. Chem. B* **2018**, *122*, 6431; b) T. Stangl, P. Wilhelm, D. Schmitz, K. Remmerssen, S. Henzel, S. S. Jester, S. Höger, J. Vogelsang, J. M. Lupton, *J. Phys. Chem. Lett.* **2015**, *6*, 1321.
[28] D. Beljonne, G. Pourtois, C. Silva, E. Hennebicq, L. M. Herz, R. H. Friend, G. D. Scholes, S. Setayesh, K. Müllen, J. L. Brédas, *Proc. Natl. Acad. Sci. USA* **2002**, *99*, 10982.
[29] J. Hofkens, M. Cotlet, T. Vosch, P. Tinnefeld, K. D. Weston, C. Ego, A. Grimsdale, K. Müllen, D. Beljonne, J. L. Brédas, S. Jordens, G. Schweitzer, M. Sauer, F. De Schryver, *Proc. Natl. Acad. Sci. USA* **2003**, *100*, 13146.
[30] a) M. Orrit, *Single Mol.* **2002**, *3*, 255; b) J. M. Lupton, J. Vogelsang, *Appl. Phys. Rev.* **2021**, *8*, 041302.
[31] G. J. Hedley, T. Schröder, F. Steiner, T. Eder, F. J. Hofmann, S. Bange, D. Laux, S. Höger, P. Tinnefeld, J. M. Lupton, J. Vogelsang, *Nat. Commun.* **2021**, *12*, 1327.
[32] A. Haugeneder, M. Neges, C. Kallinger, W. Spirkl, U. Lemmer, J. Feldmann, U. Scherf, E. Harth, A. Gugel, K. Müllen, *Phys. Rev. B* **1999**, *59*, 15346.
[33] J. Yu, R. Lammi, A. J. Gesquière, P. F. Barbara, *J. Phys. Chem. B* **2005**, *109*, 10025.
[34] F. Schindler, J. M. Lupton, J. Feldmann, U. Scherf, *Adv. Mater.* **2004**, *16*, 653.
[35] a) A. Haugeneder, M. Neges, C. Kallinger, W. Spirkl, U. Lemmer, J. Feldmann, M. C. Amann, U. Scherf, *J. Appl. Phys.* **1999**, *85*, 1124; b) M. Nisoli, S. Stagira, M. Zavelani-Rossi, S. De Silvestri, P. Mataloni, C. Zenz, *Phys. Rev. B* **1999**, *59*, 11328.
[36] K. Becker, P. G. Lagoudakis, G. Gaefke, S. Höger, J. M. Lupton, *Angew. Chem., Int. Ed.* **2007**, *46*, 3450.
[37] Y. F. Zhang, S. R. Forrest, *Phys. Rev. B* **2011**, *84*, 241301.
[38] M. Reufer, J. M. Lupton, U. Scherf, *Appl. Phys. Lett.* **2006**, *89*, 141111.
[39] Y. F. Zhang, S. R. Forrest, *Phys. Rev. Lett.* **2012**, *108*, 267404.
[40] H. Kraus, S. Bange, F. Frunder, U. Scherf, C. Boehme, J. M. Lupton, *Phys. Rev. B* **2017**, *95*, 241201.
[41] S. Bange, U. Scherf, J. M. Lupton, *J. Am. Chem. Soc.* **2012**, *134*, 1946.
[42] M. Reufer, F. Schindler, S. Patil, U. Scherf, J. M. Lupton, *Chem. Phys. Lett.* **2003**, *381*, 60.
[43] S. B. Penwell, L. D. S. Ginsberg, R. Noriega, N. S. Ginsberg, *Nat. Mater.* **2017**, *16*, 1136.
[44] M. Reufer, P. G. Lagoudakis, M. J. Walter, J. M. Lupton, J. Feldmann, U. Scherf, *Phys. Rev. B* **2006**, *74*, 241201.
[45] J. Schedlbauer, P. Wilhelm, L. Grabenhorst, M. E. Federl, B. Lalkens, F. Hinderer, U. Scherf, S. Höger, P. Tinnefeld, S. Bange, J. Vogelsang, J. M. Lupton, *Nano Lett.* **2020**, *20*, 1074.
[46] K. D. Weston, M. Dyck, P. Tinnefeld, C. Müller, D. P. Herten, M. Sauer, *Anal. Chem.* **2002**, *74*, 5342.
[47] P. Wilhelm, D. Blank, J. M. Lupton, J. Vogelsang, *ChemPhysChem* **2020**, *21*, 961.
[48] R. Coehoorn, L. Zhang, P. A. Bobbert, H. van Eersel, *Phys. Rev. B* **2017**, *95*, 134202.
[49] D. L. Gin, J. K. Avlyanov, A. G. MacDiarmid, *Synth. Met.* **1994**, *66*, 169.

[50] E. J. W. List, U. Scherf, K. Müllen, W. Graupner, C. H. Kim, J. Shinar, *Phys. Rev. B* **2002**, *66*, 235203.
[51] O. V. Mikhnenko, P. W. M. Blom, T.-Q. Nguyen, *Energy Environ. Sci.* **2015**, *8*, 1867.
[52] a) H. Lin, S. R. Tabaei, D. Thomsson, O. Mirzov, P.-O. Larsson, I. G. Scheblykin, *J. Am. Chem. Soc.* **2008**, *130*, 7042; b) H. Lin, Y. Tian, K. Zapadka, G. Persson, D. Thomsson, O. Mirzov, P.-O. Larsson, J. Widengren, I. G. Scheblykin, *Nano Lett.* **2009**, *9*, 4456; c) R. Métivier, F. Kulzer, T. Weil, K. Müllen, T. Basché, *J. Am. Chem. Soc.* **2004**, *126*, 14364.
[53] a) W. J. Baker, D. R. McCamey, K. J. van Schooten, J. M. Lupton, C. Boehme, *Phys. Rev. B* **2011**, *84*, 165205; b) J. Schedlbauer, U. Scherf, J. Vogelsang, J. M. Lupton, *J. Phys. Chem. Lett.* **2020**, *11*, 5192; c) A. J. Gesquière, S. J. Park, P. F. Barbara, *J. Am. Chem. Soc.* **2005**, *127*, 9556.
[54] D. Hertel, K. Meerholz, *J. Phys. Chem. B* **2007**, *111*, 12075.
[55] J. Vura-Weis, S. H. Abdelwahed, R. Shukla, R. Rathore, M. A. Ratner, M. R. Wasielewski, *Science* **2010**, *328*, 1547.
[56] a) M. Reufer, M. J. Walter, P. G. Lagoudakis, B. Hummel, J. S. Kolb, H. G. Roskos, U. Scherf, J. M. Lupton, *Nat. Mater.* **2005**, *4*, 340; b) Y. V. Romanovskii, A. Gerhard, B. Schweitzer, U. Scherf, R. I. Personov, H. Bässler, *Phys. Rev. Lett.* **2000**, *84*, 1027.
[57] R. Zondervan, F. Kulzer, S. B. Orlinskii, M. Orrit, *J. Phys. Chem. A* **2003**, *107*, 6770.
[58] F. Steiner, J. Vogelsang, J. M. Lupton, *Phys. Rev. Lett.* **2014**, *112*, 137402.
[59] F. Steiner, J. M. Lupton, J. Vogelsang, *J. Am. Chem. Soc.* **2017**, *139*, 9787.
[60] a) A. K. Thomas, H. A. Brown, B. D. Datko, J. A. Garcia-Galvez, J. K. Grey, *J. Phys. Chem. C* **2016**, *120*, 23230; b) A. K. Thomas, J. A. Garcia, J. Ulibarri-Sanchez, J. Gao, J. K. Grey, *ACS Nano* **2014**, *8*, 10559.
[61] A. Thiessen, J. Vogelsang, T. Adachi, F. Steiner, D. Vanden Bout, J. M. Lupton, *Proc. Natl. Acad. Sci. USA* **2013**, *110*, E3550.
[62] F. Schindler, J. M. Lupton, J. Feldmann, U. Scherf, *Proc. Natl. Acad. Sci. USA* **2004**, *101*, 14695.